

Burrowing Locomotion via Crack Propagation of a Bio-inspired Soft Robot [★]

John P. Lathrop ^{*} Derek A. Paley ^{*}

^{*} *University of Maryland, College Park, MD 20742 USA (e-mail: jlathrop@umd.edu, dpaley@umd.edu).*

Abstract: Undersea burrowing of worm-like animals involves complex hybrid dynamics with continuous-time elastic and friction forces and discrete-time events that occur when a crack forms and propagates. This paper presents a state-space model of worm-inspired burrowing locomotion using discrete elastic rod theory applied to a segmented body representing the worm's body. The effects of soil and fracture mechanics are considered in the hybrid dynamics of crack propagation. Anisotropic friction inspired by bristle-like structures in biological systems allows the worm model to create stress concentrations and advance forward through the soil. Constant-volume segments change width as they stretch and compress, affecting the friction and fracture forces on the worm body. The model is controlled by changing the intrinsic length of each segment, with several peristaltic travelling-wave gaits considered. Simulations varying gait parameters show that some travelling-wave gaits allow the worm model to make faster progress. The derived state-space model permits improved control and estimation for worm-inspired robots and empirically shows how differing travelling-wave gaits affect the speed of locomotion.

Keywords: Bio-inspired, soft robot, peristalsis, travelling wave, crack propagation

1. INTRODUCTION

Burrowing animals inhabit, consume, and modify undersea sediments by consuming and shifting benthic soils as they form their burrows. Underwater burrows provide a hunting ground, habitat, and protection from predators to more than 8,000 species of *polychaetes*, bristle worms. As discussed in Merz and Woodin (2006), these worms are named for the bristles (*chaetae*) attached to each body segment. Bristles aid anchoring, sensing, and locomotion. We are particularly interested in how these bristles enable polychaete worms to burrow in marine sediments using the cyclical burrowing gaits of marine worms examined in Dorgan (2015).

Previous work in soft robotics using Discrete Elastic Rod (DER) theory (see Goldberg et al. (2019) and Scott et al. (2021)) has examined soft robotic actuation and bio-inspired models of undersea undulatory swimming locomotion. Additionally, Scott et al. (2021) studied the effect of intrinsic parameter control in actuating a soft robotic body through a fluid medium and over flat ground using stick-slip friction. Foundational work in Dorgan et al. (2008) and Dorgan (2015) in understanding the biomechanics of worm burrowing is modeled using DER theory to investigate worm-inspired soft robotic locomotion in a segmented analogue.

Leveraging an understanding of linear elastic fracture mechanics along with the anisotropic soil interactions of polychaete bristles, we study the hybrid dynamics involved in locomotion of the worm model. The crack tip position experiences discrete jumps as the stress surpasses

the critical fracture value. The position of each worm segment changes continuously in time, governed by elastic, frictional, and fracture forces. We use a Lagrangian model of the system to derive the equations of motion.

The contributions of this paper are (1) the derivation of a state-space model of burrowing motion with sliding friction, crack propagation, and constant volume segments; (2) the investigation of the use of intrinsic length control in burrowing locomotion; and (3) an examination of a worm-inspired peristaltic gait through simulations. The contributions of this work allow for analytical descriptions of hybrid burrowing motion in robotic systems and future studies in the relationship between marine soil conditions and locomotion performance.

The paper is organized as follows. Section 2 reviews DER modeling, intrinsic length control, and fracture mechanics. Section 3 introduces an anisotropic friction model and derives the state-space model of crack propagation and worm locomotion. Section 4 presents simulation results validating the worm behavior and comparing peristaltic gaits. Section 5 summarizes contributions and discusses ongoing and future work.

2. BACKGROUND

This section introduces background material central to the proposed burrowing modeling and control scheme. Discrete elastic rod theory, control of the intrinsic length of segments, and linear elastic fracture mechanics relevant to burrowing are discussed.

[★] This research is supported by ONR Grant No. N000141712063.

2.1 Discrete Elastic Rod Model

To model the soft continuum body of a polychaete worm, Discrete Elastic Rod (DER) theory (see Bergou et al. (2008), Goldberg et al. (2019)) discretizes the worm body into segments. Burrowing behavior is examined using linearly extensible, unbending segments. The rod model has N nodes and $N - 1$ segments. Shape variables with a subscript (e.g., x_k) denote *node* properties and variables with a superscript (e.g., l^k) denote *segment* properties. The value of time-varying properties at $t = 0$ are identified by subscript 0 (e.g., l_0^k).

The position and velocity of each node is denoted by x_k and v_k , respectively, for $k = 1, \dots, N$. Node $k = 1$ is the head of the worm and node $k = N$ is the tail. The length of the k^{th} segment is $l^k = x_k - x_{k+1}$. Assume $x_k > x_{k+1}$ and equivalently $l^k > 0$ for all $k = 1, \dots, N - 1$. The initial length of the k^{th} segment is l_0^k . The width of the k^{th} segment is w^k and the initial width w_0^k . The initial widths and lengths of all segments are identical.

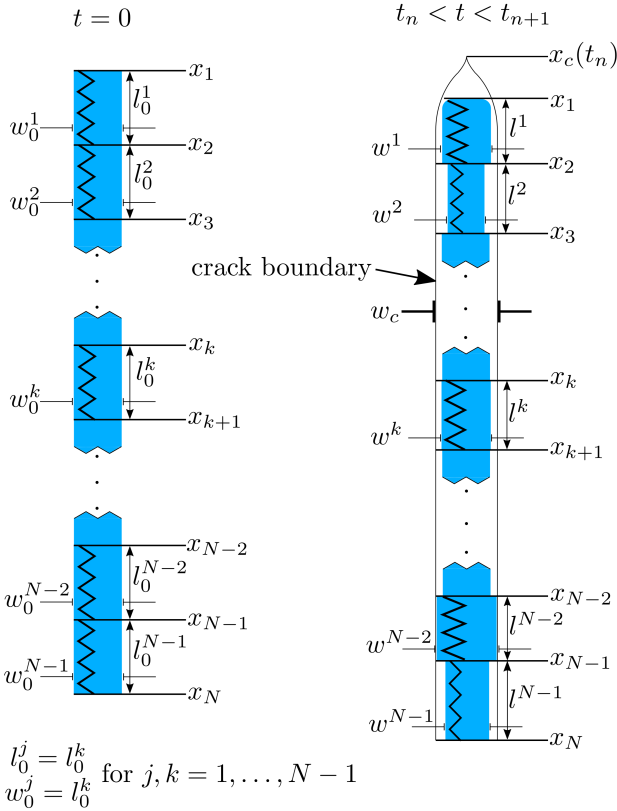


Fig. 1. The worm model is discretized into N nodes connected by $N - 1$ linearly elastic segments. The variables x_1, x_2, \dots, x_N are the node positions. The length and width of each segment k is denoted as l^k and w^k for $k = 1, \dots, N - 1$, respectively. (Left) The unstretched initial worm position, with equal segment lengths (l_0^k) and widths (w_0^k); (Right) the worm in motion, with variable segment widths. The crack tip x_c is in front of the worm's head; the crack propagation times are denoted t_n .

The mass of segment k is $m^k = m$ for all $k = 0, \dots, N - 1$. The mass m_k of node k is found by distributing the mass of each segment to each node it adjoins, with $m_1 = m_N = m/2$ and $m_k = m$ for $k = 2, \dots, N - 1$. Following Dorgan et al. (2006), the volume V_{const} of each segment is constant during peristalsis.

The position of the crack tip is denoted x_c . The constant width of the crack profile is w_c . Assume the worm and crack have the same out-of-plane thickness h .

The resting position of the worm model in the absence of external forces is defined by the intrinsic length \bar{l}^k of each segment. For an unstretched worm at rest, the length of each segment matches, i.e., $l^k = \bar{l}^k$. The stretching stiffness of each worm segment is the product of its elasticity and the segment area and denoted as EA .

To derive the equations of motion, we use a Lagrangian approach, following Goldberg et al. (2019). The total kinetic energy T is

$$T = \frac{1}{2} \sum_{k=1}^N m_k \dot{x}_k^2 = \frac{1}{4} m \dot{x}_1^2 + \frac{1}{2} \sum_{k=2}^{N-1} m \dot{x}_k^2 + \frac{1}{4} m \dot{x}_N^2 \quad (1)$$

and the stretching potential energy V is

$$\begin{aligned} V &= \frac{1}{2} EA \sum_{k=1}^{N-1} \bar{l}^k \left(\frac{l^k}{\bar{l}^k} - 1 \right)^2 \\ &= \frac{1}{2} EA \sum_{k=1}^{N-1} \frac{(x_k - x_{k+1} - \bar{l}^k)^2}{\bar{l}^k}. \end{aligned} \quad (2)$$

Using the standard Lagrangian $\mathcal{L} = T - V$, Lagrange's equation $\frac{d}{dt} \frac{\partial \mathcal{L}}{\partial \dot{x}_k} - \frac{\partial \mathcal{L}}{\partial x_k} = Q_k$ yields the following equations of motion:

$$\begin{aligned} \frac{1}{2} m \ddot{x}_1 + EA \left(\frac{x_1 - x_2}{\bar{l}^1} - 1 \right) &= Q_1 \\ m \ddot{x}_k + EA \left(\frac{x_k - x_{k+1}}{\bar{l}^k} - \frac{x_{k-1} - x_k}{\bar{l}^{k-1}} \right) &= Q_k \\ \frac{1}{2} m \ddot{x}_N + EA \left(1 - \frac{x_{N-1} - x_N}{\bar{l}^{N-1}} \right) &= Q_N, \end{aligned} \quad (3)$$

where $k = 2, \dots, N - 1$.

The generalized, non-conservative forces Q_1 , Q_k , and Q_N are derived in Section 3. Note, there is no bending or twisting energy in the worm model.

2.2 Intrinsic Length Control

Introduced in Scott et al. (2021), a practical control scheme for actuating soft robotic structures is intrinsic parameter control. Here, the control input is the time rate of change of the intrinsic lengths $\bar{l} = [\bar{l}^1, \dots, \bar{l}^{N-1}]$. Intrinsic length control mimics the muscular contraction and changing pressure of the body fluid of worm and worm-like animals that change their shape (see Chapman (1950) and Quillin (1998)).

The control scheme defines the rate of change of intrinsic length as $\dot{l} = \mathbf{u}$. The control input \mathbf{u} may be designed using open-loop or closed-loop control. The benefits of closed-loop control on soft robotic locomotion are in the rejection of disturbances arising from unmodeled external forces and sensor noise.

Another benefit of modeling the input as the rate of change \dot{l} of the intrinsic length is the stretching potential. The control input does not appear explicitly in the potential energy, which is a function of the state variables. Additionally, the rate of change of intrinsic length mimics the pump fluid flow rate in a physical bellows-style fluidic actuator (see Scott et al. (2021)).

2.3 Worm-Soil Interactions and Fracture Mechanics

We analytically study the growth of cracks in marine soils to characterize how undersea animals burrow using linear elastic fracture mechanics. To characterize marine soil, consider the soil's modulus of elasticity E_s , Poisson's ratio ν , and fracture constants K_{Ic} and K_{Ith} .

Additionally, we examine the interface between worms and soil. Polychaete worms have outward-facing bristles that serve a multitude of functions (Merz and Woodin (2006)). Hooked-shaped and mobile bristles enable burrowing of polychaete worms using anisotropic friction.

These marine fauna exert fracture forces around their heads to open cracks, called Mode I loading (Dorgan et al. (2008)). Accumulated stress results in crack propagation. By advancing forward into cracks using a four-stage gait, an undersea animal creates a burrow. As described in Dorgan (2015), the four stages of burrowing in a marine worm are (i) the worm advances to the front of the crack; (ii) the worm pushes its head forward to propagate the crack; (iii) the worm thickens its segments to widen the crack; and (iv) a peristaltic travelling wave advances the body while the head slips back.

For small length and time scales (Dorgan et al. (2007)), linear elastic fracture mechanics are applicable to burrowing behavior. The stress concentration factor K_I characterizes the accumulation of stress at crack tips, with the subscript I denoting stress concentrations as a result of Mode I loading. We examine two specific values of K_I : the critical stress intensity factor K_{Ic} and the threshold stress intensity factor K_{Ith} . The critical value K_{Ic} is the upper limit of stress concentration before unstable crack propagation begins. The threshold value K_{Ith} is the lower threshold of stress concentrations, below which crack propagation ceases to occur.

From Dorgan et al. (2008), the time-varying stress intensity factor K_I due to a worm acting as a wedge at the tip of a crack is

$$K_I(t) = \frac{E_s w^1}{\sqrt{2\pi(x_c(t_n) - x_1(t))(1 - \nu^2)}}, \quad (4)$$

where we have used the profile of a square-headed worm.

As discussed in Dorgan (2015), soil conditions and burrowing behavior of marine worms is characterized by the

dimensionless wedge number denoted in literature as Wg . Let $G_c = K_{Ic}^2/E_s$ denote the fracture toughness. We have

$$Wg = \frac{W_{fracture}}{W_{elastic}} = \frac{G_c w_c}{E_s h w_0^1} = \frac{K_{Ic}^2 w_c}{E_s^2 h w_0^1}. \quad (5)$$

3. BURROWING MODEL

This section derives a state-space model of burrowing locomotion. Included in this model are anisotropic friction effects, linear elastic fracture mechanics, and the effect of crack tip position on the worm itself. Simulation results of worm locomotion and crack propagation are included to illustrate the model behavior.

3.1 Anisotropic Friction Model

Considering a constant friction coefficient, let μ_s be the coefficient of sliding friction. Let λ be the frictional coefficient multiplier that causes increased friction opposing backwards motion.

For a given crack width w_c , the displacement of the soil around the k^{th} segment depends on the width w^k of the k^{th} segment. For a constant segment volume, w^k depends on the length of the k^{th} segment, $l^k = x_k - x_{k+1}$. Using the initial length l_0^k of the k^{th} segment and a constant planar thickness h , we have $V_{const} = w_0^k l_0^k h = w^k l^k h$, which implies

$$w^k = w_0^k \frac{l_0^k}{l^k} = \frac{w_0^k l_0^k}{x_k - x_{k+1}}. \quad (6)$$

When the width of the k^{th} segment exceeds the constant crack width w_c , a normal stress develops on the segment. For segments thinner than w_c , no stress develops. As the soil is linearly elastic, the force exerted on the worm segments is proportional to the displacement of the soil. The normal stress σ_N^k and the normal force F_N^k on the k^{th} segment are

$$\sigma_N^k = \max \left\{ E_s \left[\frac{w_0^k l_0^k}{x_k - x_{k+1}} - w_c \right], 0 \right\}, \quad (7)$$

$$\begin{aligned} F_N^k &= (x_k - x_{k+1}) h \max \left\{ E_s \left[\frac{w_0^k l_0^k}{x_k - x_{k+1}} - w_c \right], 0 \right\} \\ &= \max \{ E_s h (w_0^k l_0^k - w_c [x_k - x_{k+1}]), 0 \}. \end{aligned} \quad (8)$$

Since $(x_k - x_{k+1})h > 0$, we can move this expression inside the max function.

Equation (8) shows that the normal force on the k^{th} segment is a function of the state variables x_k and x_{k+1} , and affected by the soil elasticity E_s , planar worm thickness h , original worm width w_0^k , original segment length l_0^k , and crack width w_c .

For the derivation of the frictional forces, the velocity v^k of the k^{th} segment is the average velocity of the surrounding nodes, i.e.,

$$v^k = \frac{v_k + v_{k+1}}{2} = \frac{\dot{x}_k + \dot{x}_{k+1}}{2}. \quad (9)$$

The sliding friction on the k^{th} segment opposes the direction of motion. When the k^{th} segment is moving backwards, the friction coefficient is $\lambda\mu_s$, whereas when the k^{th} segment is moving forward, the friction coefficient is μ_s . The force of friction is

$$F_f^k = \mu_s \left[\frac{\lambda - 1}{2} - \frac{\lambda + 1}{2} \text{sgn}(v^k) \right] F_N^k, \quad (10)$$

where $\text{sgn}(\cdot)$ denotes the signum function.

The friction acting on the k^{th} node is half that acting on each adjacent segment. The first node has a friction contribution from only the segment $k = 1$, and the last node from only $k = N - 1$:

$$\begin{aligned} F_{f,1} &= \frac{F_f^1}{2} \\ F_{f,k} &= \frac{F_f^{k-1} + F_f^k}{2} \text{ for } k = 2, \dots, N-1 \\ F_{f,N} &= \frac{F_f^{N-1}}{2}. \end{aligned} \quad (11)$$

3.2 Crack Propagation Model

Recall K_{Ic} is the critical stress intensity factor that determines when crack propagation occurs and K_{Ith} is the threshold stress intensity factor below which crack propagation does not occur. Both quantities are constant properties of the soil.

When the stress intensity factor $K_I(t)$ rises above the critical value K_{Ic} , the crack propagates forward until $K_I(t)$ falls below the threshold value K_{Ith} . Let t_n denote the time of the n^{th} crack propagation, for $n = 1, 2, \dots$. Adapting (4) for constant volume (and variable width) worm segments using (6) yields

$$K_I(t) = \frac{E_s w_0^1 l_0^1}{\sqrt{2\pi(x_c(t_n) - x_1(t))(1 - \nu^2)(x_1(t) - x_2(t))}}. \quad (12)$$

When $K_I(t)$ exceeds K_{Ic} , the crack tip advances until $K_I(t) = K_{Ith}$. The new crack position is found by equating these quantities and solving for $x_c(t_{n+1})$:

$$x_c(t_{n+1}) = x_1(t_n) + \frac{E_s^2 (w_0^1)^2 (l_0^1)^2}{2\pi K_{Ith}^2 (1 - \nu^2)^2 (x_1(t_n) - x_2(t_n))^2}. \quad (13)$$

To model the force of the soil on the head of the worm, i.e., the soil back pressure, consider the dimensionless wedge ratio Wg from (5).

From linear elastic fracture mechanics, the stress $\sigma(t)$ resulting from stress intensity factor K_I at a distance r from the crack tip is

$$\sigma(t) = \frac{K_I(t)}{\sqrt{2\pi r}} f \quad (14)$$

for a shape factor f . The force is the product of the contact area and the stress on the contact area. Using Wg to relate

the fracture and elastic work, the soil back pressure caused by fracturing is

$$\begin{aligned} F_p(t) &= \frac{K_I(t)}{\sqrt{2\pi(x_c(t_n) - x_1(t))}} Wg w^1 h \\ &= \frac{K_I(t)}{\sqrt{2\pi(x_c(t_n) - x_1(t))}} Wg \frac{w_0^1 l_0^1}{x_1(t) - x_2(t)} h \end{aligned} \quad (15)$$

for $t_n < t < t_{n+1}$. Here, the blunt head of the worm is the contact area $w^1 h$ that the stress acts on. Rewriting (15) using (12) yields

$$F_p(t) = \frac{E_s (w_0^1)^2 (l_0^1)^2 h Wg}{2\pi(x_c(t_n) - x_1(t))(x_1(t) - x_2(t))^2 (1 - \nu^2)} \quad (16)$$

for $t_n < t < t_{n+1}$.

3.3 State Space Model

Recalling the equations of motion (3), we equate the sum of the frictional (11) and soil back pressure (16) forces with the generalized forces Q_1, Q_2, \dots, Q_N . The equations of motion are

$$\begin{aligned} \frac{1}{2} m \ddot{x}_1 + EA \left(\frac{x_1 - x_2}{l^1} - 1 \right) &= F_{f,1} - F_p \\ m \ddot{x}_k + EA \left(\frac{x_k - x_{k+1}}{l^k} - \frac{x_{k-1} - x_k}{l^{k-1}} \right) &= F_{f,k} \\ \frac{1}{2} m \ddot{x}_N + EA \left(1 - \frac{x_{N-1} - x_N}{l^{N-1}} \right) &= F_{f,N} \end{aligned} \quad (17)$$

for $k = 2, \dots, N - 1$.

Let $\mathbf{x} = [x_1, x_2, \dots, x_N]^T$ and $\dot{\mathbf{x}} = [\dot{x}_1, \dot{x}_2, \dots, \dot{x}_N]^T$. We have $\ddot{\mathbf{x}} = h(\mathbf{x}, \dot{\mathbf{x}}, \bar{\mathbf{l}}, x_c)$, where

$$h(\mathbf{x}, \dot{\mathbf{x}}, \bar{\mathbf{l}}, x_c) = -\mathcal{M}^{-1}(\mathcal{V}_s(\mathbf{x}, \bar{\mathbf{l}}) - \mathcal{F}_f(\mathbf{x}, \dot{\mathbf{x}}) + \mathcal{F}_p(\mathbf{x}, x_c)) \quad (18)$$

$$\mathcal{M}^{-1} = \begin{bmatrix} \frac{2}{m} & 0 & 0 & \cdots & 0 & 0 \\ 0 & \frac{1}{m} & 0 & \cdots & 0 & 0 \\ 0 & 0 & \frac{1}{m} & \cdots & 0 & 0 \\ \vdots & \vdots & \vdots & \ddots & 0 & 0 \\ 0 & 0 & 0 & \cdots & \frac{1}{m} & 0 \\ 0 & 0 & 0 & \cdots & 0 & \frac{2}{m} \end{bmatrix} \quad (19)$$

$$\mathcal{V}_s(\mathbf{x}, \bar{\mathbf{l}}) = \begin{bmatrix} EA \left(\frac{x_1 - x_2}{l^1} - 1 \right) \\ \vdots \\ EA \left(\frac{x_k - x_{k+1}}{l^k} - \frac{x_{k-1} - x_k}{l^{k-1}} \right) \\ \vdots \\ EA \left(1 - \frac{x_{N-1} - x_N}{l^{N-1}} \right) \end{bmatrix} \quad (20)$$

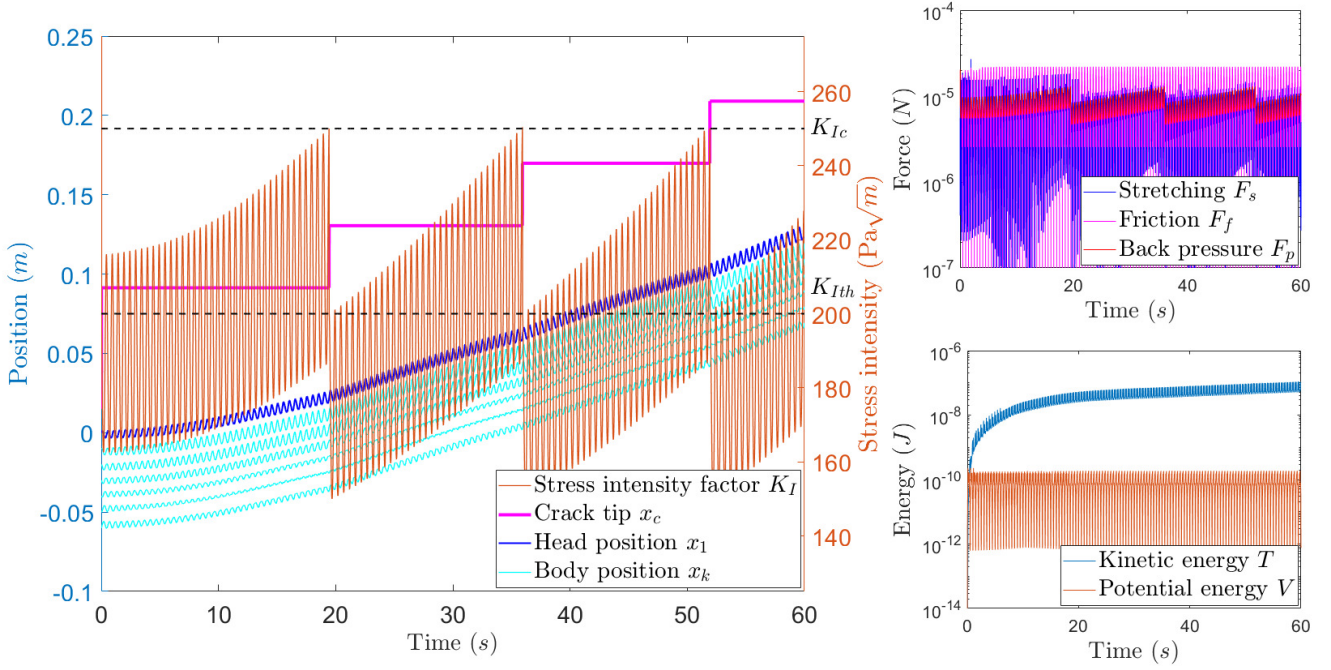


Fig. 2. Left: Relationship between crack tip position (magenta), worm head position (blue), worm body positions (cyan), and stress intensity factor (orange). Black dotted lines indicate the critical and threshold values of K_I . When K_I overcomes the critical value, the crack advances. Upper right: Stretching forces (blue), frictional forces (magenta), and back-pressure forces (red). Lower right: Kinetic energy (blue) and stretching potential energy (orange).

$$\mathcal{F}_f(\mathbf{x}, \dot{\mathbf{x}}) = \begin{bmatrix} \frac{1}{2}\mu_s \left[\frac{\lambda-1}{2} - \frac{\lambda+1}{2} \operatorname{sgn}\left(\frac{\dot{x}_1 + \dot{x}_2}{2}\right) \right] \max\{E_s h(w_0^1 l_0^1 - w_c[x_1 - x_2]), 0\} \\ \vdots \\ \frac{1}{2}\mu_s \left[\frac{\lambda-1}{2} - \frac{\lambda+1}{2} \operatorname{sgn}\left(\frac{\dot{x}_{k-1} + \dot{x}_k}{2}\right) \right] \max\{E_s h(w_0^{k-1} l_0^{k-1} - w_c[x_{k-1} - x_k]), 0\} \\ + \frac{1}{2}\mu_s \left[\frac{\lambda-1}{2} - \frac{\lambda+1}{2} \operatorname{sgn}\left(\frac{\dot{x}_k + \dot{x}_{k+1}}{2}\right) \right] \max\{E_s h(w_0^k l_0^k - w_c[x_k - x_{k+1}]), 0\} \\ \vdots \\ \frac{1}{2}\mu_s \left[\frac{\lambda-1}{2} - \frac{\lambda+1}{2} \operatorname{sgn}\left(\frac{\dot{x}_{N-1} + \dot{x}_N}{2}\right) \right] \max\{E_s h(w_0^{N-1} l_0^{N-1} - w_c[x_{N-1} - x_N]), 0\} \end{bmatrix} \quad (21)$$

$$\mathcal{F}_p(\mathbf{x}, x_c) = \begin{bmatrix} \frac{E_s (w_0^1)^2 (l_0^1)^2 h W g}{2\pi (x_c - x_1)(x_1 - x_2)^2 (1 - \nu^2)} \\ 0 \\ \vdots \\ 0 \end{bmatrix} \quad (22)$$

for $k = 2, \dots, N-1$.

Let $\mathbf{q} = [\mathbf{q}_1, \mathbf{q}_2]^T = [\mathbf{x}, \dot{\mathbf{x}}]^T$. The first-order state-space dynamics with intrinsic length control \mathbf{u} are

$$\dot{\mathbf{q}} = \begin{bmatrix} \mathbf{q}_2 \\ h(\mathbf{q}, \dot{\mathbf{l}}, x_c) \end{bmatrix} \quad (23)$$

$$\dot{\mathbf{l}} = \mathbf{u}.$$

4. SIMULATION RESULTS

This section illustrates the behavior of the burrowing model and studies locomotion performance. We integrate

the state-space dynamics in MATLAB using an implicit backwards Euler solver, using the representative simulation parameters shown in Table 1.

As discussed in Section 2.2, we actuate the system dynamics with intrinsic length control. Consider an open-loop travelling-wave gait, where the rate of change of the intrinsic length $\dot{\mathbf{l}}$ follows a sinusoidal function of a phase variable $\psi_k(t)$. The control input \mathbf{u} is (Scott et al. (2021))

$$\mathbf{u}(t) = [A \sin(\psi_1(t)) \quad A \sin(\psi_2(t)) \quad \dots \quad A \sin(\psi_N(t))], \quad (24)$$

and the phase variable $\psi_k(t)$ is (Scott et al. (2021))

$$\psi_k(t) = \omega t + \delta k, \quad (25)$$

where δ is the phase offset between nodes of the gait.

The simulated worm uses peristaltic motion to advance forward in the crack. Crack propagation occurs when the stress intensity factor K exceeds the critical value K_{Ic} . As

Table 1. Model Simulation Parameters

Parameter	Value	Units
Number of nodes (N)	7	-
Soil elasticity (E_s)	1.4×10^5	Pa
Critical stress intensity factor (K_{Ic})	250	$\text{Pa}\sqrt{\text{m}}$
Threshold stress intensity factor (K_{Ith})	200	$\text{Pa}\sqrt{\text{m}}$
Poisson's ratio (ν)	0.3	-
Crack width (w_c)	0.001	m
Wedge number (Wg)	4.59×10^{-4}	-
Stretching stiffness (EA)	13	$\text{Pa}\cdot\text{m}^2$
Unstretched segment width (w_0^k)	0.001	m
Unstretched segment length (l_0^k)	0.01	m
Planar thickness (h)	0.001	m
Mass per segment (m^k)	10^{-5}	kg
Sliding friction coefficient (μ_s)	0.3	-
Friction coefficient multiplier (λ)	1.5	-
Gait amplitude (A)	0.02	m/s
Gait angular frequency (ω)	4π	rad/s
Gait offset (δ)	$\pi/4$	rad

shown in Figure 2, the crack tip advancement coincides with forward progress of the worm head that results in increased stress intensity factor.

4.1 Locomotive Parameter Study

To further study the burrowing model and control scheme, we simulated worm locomotion over 60 seconds for a range of gait parameters. The gait amplitude $A = 0.02$ m/s was held constant while the angular frequency ω was varied between 3π and 5π and offset δ was varied between $\pi/6$ and $\pi/3$. The speed of the center of mass was calculated over the 60 second period and plotted in Figure 3.

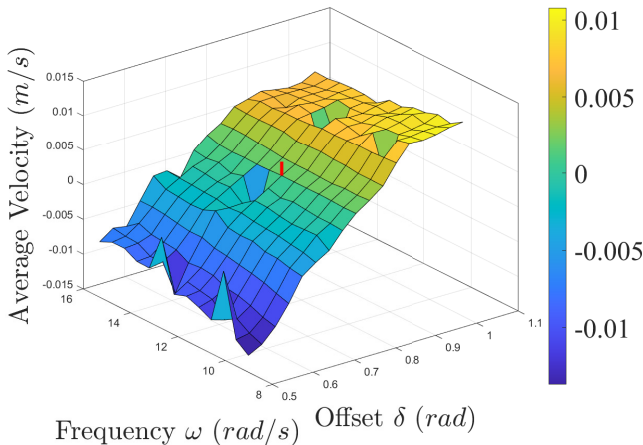


Fig. 3. The average velocity varies for gait frequencies and offsets described in Section 4.1. The red tick mark in the center of the figure indicates the simulation shown in Figure 2, with average velocity 0.0022 m/s.

For the range of values examined, the velocity of locomotion increases with increasing offset δ . Values of δ below approximately $\delta = 0.74$ caused the center of mass of the worm to travel backwards, retreating out of the crack. The fastest forward-progressing simulation ($v = 0.0108$ m/s) arose from the lowest frequency, $\omega = 3\pi$, and the largest offset, $\delta = \pi/3$. The fastest retreating simulation ($v = -0.0137$ m/s) occurred for $\omega = 3\pi$ and $\delta = \pi/6$.

Lower travelling-wave frequencies ω caused faster locomotion regardless of the direction of travel. Lower frequencies caused the model worm to either advance into the crack or extract itself at a higher speed. The fastest travel wave frequencies examined, $\omega = 5\pi$, caused slower overall locomotion than the slower frequencies examined. Though the model still made nonzero progress for values of δ near $\pi/3$ and $\pi/6$, the velocity was constrained between -0.005 m/s and 0.005 m/s, a factor of two slower than $\omega = 3\pi$.

5. CONCLUSION

This paper presents a state-space model of burrowing locomotion for a worm-inspired segmented robot. The model includes anisotropic friction inspired by polychaete worms and linear elastic fracture mechanics. Simulations of worm model locomotion exhibit the cyclical relationship between crack propagation and the progress of the worm. Each segment has constant volume. The widths contract and expand as the lengths are driven by phase-shifted sinusoidal input representing the travelling wave characteristics of peristaltic locomotion. Ongoing and future research aims to further study how changing gait parameters A , ω , and δ permits faster and more energy-efficient locomotion. Soil parameters E_s , K_{Ic} , and K_{Ith} and wedge number Wg also affect the speed of locomotion and energy loss due to friction.

REFERENCES

- K.M. Dorgan, S.R. Arwade, P.A. Jumars. Worms as wedges: effects of sediment mechanics on burrowing behavior. *J. of Marine Research*, 66:219–254, 2008.
- K.M. Dorgan, S.R. Arwade, P.A. Jumars. Burrowing in marine muds by crack propagation: kinematics and forces. *J. of Experimental Biology*, 210:4198–4212, 2007.
- N.N. Goldberg, X. Huang, C. Majidi, A. Novelia, O.M. O'Reilly, D.A. Paley, W.L. Scott. On planar discrete elastic rod models for the locomotion of soft robots *Soft Robotics*, 6:5, 2019.
- K.M. Dorgan, P.A. Jumars, B.D. Johnson, B.P. Boudreau. Macrofaunal burrowing: the medium is the message. *Oceanography and Marine Biology*, 44:85–121, 2006.
- W.L. Scott, P.J. Prakash, D.A. Paley. Distributed control of a planar discrete elastic rod for eel-inspired underwater locomotion. In D.A. Paley, N.M. Wereley (ed.). *Bioinspired sensing, actuation, and control in underwater soft robotic systems*. pp. 261–279. Springer Intl., Cham, CH, 2021. <https://doi.org/10.1007/978-3-030-50476-2>
- R.A. Merz, S.A. Woodin. Polychaete chaetae: function, fossils, and phylogeny. *Integrative and Comparative Biology*, 46:481–496, 2006.
- M. Bergou, M. Wardetzky, S. Robinson, B. Audoly, E. Grinspun. Discrete elastic rods. *ACM Trans. Graph.*, 2008.
- K.M. Dorgan. The biomechanics of burrowing and boring. *J. of Experimental Biology*, 218:176–183, 2015.
- G. Chapman. Of the movement of worms. *J. of Experimental Biology*, 27:29–39, 1950.
- K.J. Quillin. Ontogenetic scaling of hydrostatic skeletons: geometric, static stress and dynamic stress scaling of the earthworm lumbricus terrestris. *J. of Experimental Biology*, 201:1871–1883, 1998.